MASSACHUSETTS INSTITUTE OF TECHNOLOGY

LINCOLN LABORATORY

RADAR OBSERVATIONS OF THE MOON AT 8.6-mm WAVELENGTH

V. L. LYNN

M. D. SOHIGIAN

E. A. CROCKER

Group 45

TECHNICAL REPORT NO. 331

8 OCTOBER 1963

LEXINGTON MASSACHUSETTS

ABSTRACT

The experimental, pseudo-CW radar used to detect the first lunar echoes at millimeter wavelengths is described. This system, with a peak-power output of 12 watts, has been used to obtain preliminary mapping of the moon at a wavelength of 8.6 mm with resolution in angle only.

Approximately 85 percent of the reflected power can be attributed to diffuse scattering. This component appears to follow the Lommel-Seeliger Law although there are insufficient data to define the distribution accurately. For the positions observed, there was no significant difference in reflection between the maria and the continents, within limits of approximately ± 2 db.

The total radar cross section of the moon at 8.6-mm wavelength was determined to be 7 ± 2 percent of the geometric cross section.

This technical documentary report is approved for distribution.

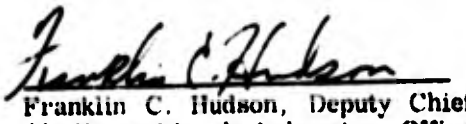

Franklin C. Hudson, Deputy Chief
Air Force Lincoln Laboratory Office

RADAR OBSERVATIONS OF THE MOON AT 8.6-mm WAVELENGTH

I. INTRODUCTION

The advantages of the millimeter-wavelength band in many applications are numerous and have been outlined in detail by several workers. Principal among these are the characteristic wide bandwidths, unused spectrum, small size of components, and high angular resolution with antennas of modest size. In the early days of radar, frequencies were quickly pushed toward the water vapor absorption line at 25 Gcps and then reverted, for the most part, to wavelengths of X-band and longer. At that time when virtually all radar and communications systems operated on essentially horizontal paths, the loss of 2 db on a 10-mile transmission in dry weather, with considerably worse effects under storm conditions, was sufficient to render the millimeter band unusable in operational situations. For this reason, little component development was undertaken for several years and the state of the art considerably lagged that which might be scaled from lower frequencies. Now, however, with the advent of extraterrestrial radar and communications requirements, a renewed interest in the band has developed. Even for an earth-based terminal, the limitations of absorption are much less severe. At 35 Gcps (8.6-mm wavelength), the first "window", the total loss incurred under dry conditions on a vertical path through the atmosphere is approximately 0.2 db, while at 95 Gcps (3.2-mm), the second absorption minimum, the comparable loss is about 1 db (Ref. 1). These values and the higher ones resulting from precipitation and non-zenith angles can be greatly mitigated by a judicious choice of climate or the use of elevated locations for the terrestrial terminals.

With this new attractiveness of the millimeter band, Lincoln Laboratory initiated a program of space-oriented systems and component development. The final testing of very long range radar and communications systems becomes, in itself, a difficult problem for frequency ranges where componentry is not fully developed and performance is relatively low. It is possible, of course, to utilize satellites and rockets as targets or communication stations. However, this is expensive and has limited duration of utilization. Under these circumstances, it was decided to construct a radar system capable of observing reflections from the moon – a stable, and at least partially predictable, target of varied parameters. As a radar reflector, the moon is relatively large when considered in toto. However, for a narrow antenna beamwidth such as used in the experiments described herein, the effective cross section observed is approximately equivalent to one square meter at a thousand miles. If one considers this radar path as a communications link wherein the single station is communicating with itself, the lunar radar is effectively a pair of terminals utilizing identical antennas and separated by more than ten times the distance to the planet Pluto.

In addition to the admirable characteristics as a pure test range, the lunar observations offer the possibility of valuable physical measurements. Previous radar observations have been made only at wavelengths of 3 cm and longer. At 8.6 mm and shorter wavelengths, any carefully taken data can contribute significantly toward knowledge of selenographic characteristics. In particular, there is the capability of making one type of observation that has not been possible in previous experiments – the measurement of reflective properties using resolution in angle only. At lower frequencies, radars generally resolve the lunar surface in range and doppler, while in radiometric observations of lunar emission, the antenna beams are generally such that each measurement represents integration over a major fraction of the surface. For this reason, direct comparison of active and passive data for a specific location has not been possible heretofore, and both have been treated separately. Such a direct comparison appears to be highly desirable and will be possible in the millimeter band.

First detection of 8.6-mm radar echoes was accomplished in April 1963 (Ref. 2), and in May 1963 a moderately extensive observational program was undertaken. It is the intent of this report to describe the equipment used in these tests and the results obtained. There are a number of areas in which easily implemented improvements will occur to the reader, primarily because the radar was designed principally to permit detection rather than to make precise measurements. Obvious among these are increased transmitter power (available since the tests described), lower receiver-noise temperature, inclusion of doppler and range resolution, polarization diversification and the correction of non-conceptual equipment weaknesses. It is anticipated that all of these improvements will be incorporated in advanced versions of this system to permit more thorough measurements. This report will be confined to a description of the radar prior to modification.

II. EQUIPMENT

A. Antenna

Figure 1 shows the precision 28-foot diameter antenna installed on the roof of Lincoln Laboratory. A length of oversize circular waveguide, operating in the TE_{11} mode, runs from the equipment housing at the rear of the vertex to a point several wavelengths from a 5-inch-diameter,

Fig. 1. 28-foot precision antenna on the roof of Lincoln Laboratory.

flat, circular secondary reflector near the focal point. This feed system can be described by Cassegrainian optics.[3]

A permanently installed pattern-measurement range is an integral part of this antenna system. Using this range the performance of the antenna under varying conditions has been extensively evaluated. The methods and results are described in detail elsewhere.[4]

To permit focussing of the antenna without the use of flexible waveguide or movable joints, all microwave components of the radar and pattern receiver are mounted on a single large plate in the equipment housing. Adjustment is accomplished by movement of the entire plate and feed. Since the pattern range is equivalent in length to only $1.15\ D^2/\lambda$ (the remote transmitter is at a distance of 31,500 feet), there is a slight defocus introduced when the position produces the optimum patterns on this range. The change in feed position necessary to correct for far-field observation is automatically accomplished by connection of the radar system through a precise differential position of the appropriate components.

The parameters which describe the performance of this antenna with the best estimates of uncertainty are:

Gain above isotropic	67.5 ± 0.5 db
Effective area	31.5 ± 1.5 m^2
Half-power beamwidth	4.3 ± 0.1 mins arc
Aperture efficiency	55 ± 5 percent
Feed line loss	1.4 ± 0.1 db
Cross polarized pattern below peak gain	>20 db
Polarization	Horizontal

The one-way plane patterns of Fig. 2 were taken at night to avoid variations in sidelobe levels observed under conditions of solar heating. Figure 3, a three-dimensional representation of the radiation pattern, was plotted from data taken on a bright, sunny day and is a typical example

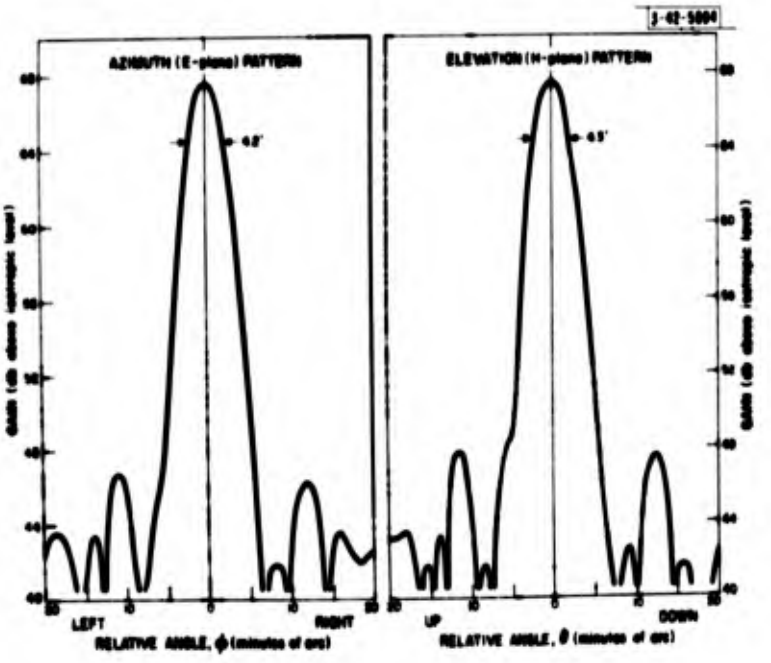

Fig. 2. Antenna directional diagram in principal planes.

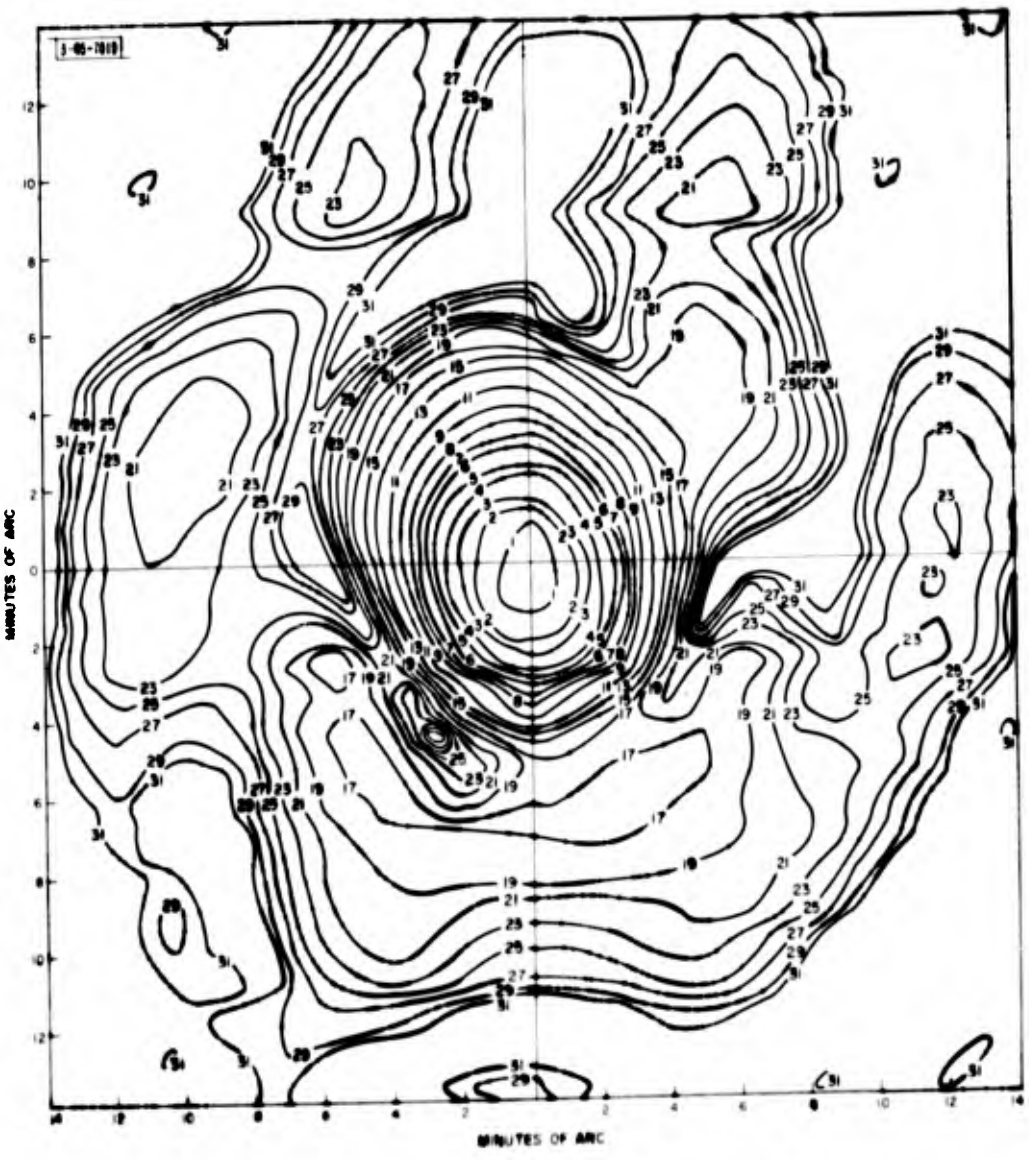

Fig. 3. Polar contour plot of antenna pattern as taken on bright, sunny day. Contours are labeled in db below peak gain.

of the effect of such conditions. All lunar observations were made at night although, in spite of the pattern asymmetry under sunny conditions, there is no change in either gain or half-power beamwidth from that observed at night. In the reduction of data, the circularly symmetric equivalent of the pattern was derived by planimeter integration of the contours of the solid angle plot. The result shown in Fig. 4, while obviously not descriptive of the directivity characteristics, allows a precise correction of data for beam geometry after the method of Evans and Pettengill.[5]

B. Pointing and Control

The antenna is mounted on an azimuth-elevation drive system which is, unfortunately, inadequate to permit the use of position-servo drives. The prime method of directing the beam, and that which was used in the radar observations, is manual control of rate-feedback-servo loops with reference to a boresighted-television system. Prior to every series of tests, the boresighting was checked by electrically aiming the center of the beam at the range transmitter and then aligning the telescope-television system to be parallel, using a high-intensity light which was offset to correct for parallax.

To avoid errors due to inaccurate gearing and flexibility of the mount base, the 6-inch lens system and television camera were installed directly on the reflector backup structure, the

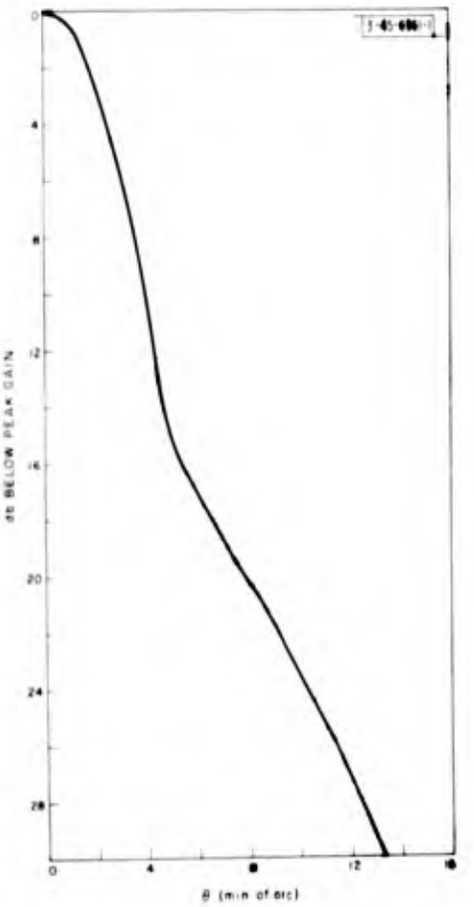

Fig. 4. Equivalent pattern of symmetry.

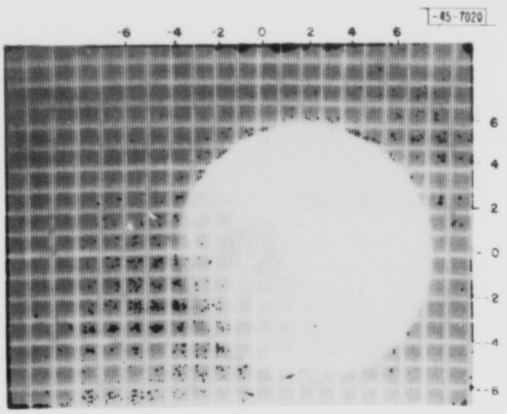

Fig. 5. Television boresight monitor showing grid and moon.

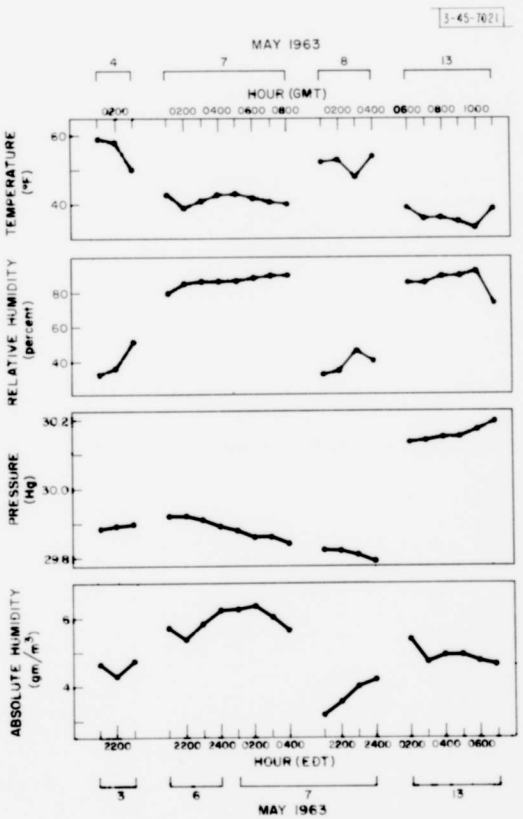

Fig. 6. Meteorological conditions at ground level during observations.

controlling operators viewing through a hole in the reflector. The rate-servo controls and television monitor were located in a nearby building along with the other non-microwave portions of the radar.

The telescope-television system was of poor quality and, consequently, only the gross lunar features could be distinguished in the display. With an antenna two-way beamwidth approximately equivalent to one-tenth of the lunar diameter, it was necessary to direct the antenna to a fraction of one minute of arc in order to obtain useful data. Therefore, a rectilinear-gridded reticle was installed in the optical system with grid spacing equivalent to 2.5'. Figure 5 shows the display with the moon in the field of view. To accurately define the beam position on the lunar surface, the circular portion of the moon image was maintained tangent to two specific grid lines for a given run. The rate of drive was then adjusted to maintain track at that position.

C. Radar System

The radar is basically a very-low-power, long-pulse system dependent on a high degree of frequency stability and high antenna gain for the achievement of performance. A detailed description of the operation of the radar is given in Appendix A. Table I summarizes the system and propagation parameters as they occurred during the May 1963 observations.

III. EXPERIMENTAL PROCEDURES

Each evening of operation, several series of calibration recordings were made with various levels of input. All pertinent radar parameters were measured in absolute terms before and after the observations and monitored for change during the tests.

Forty series of measurements of lunar reflection were made for different selenographic positions. Each series consisted of recording 20 to 40 valid pulses with the beam directed at a specific point. On any given day, each transmitted pulse was assigned (consecutively) a number. Many pulses occurred between data runs and, within a run, some were discarded for various reasons. Predominant among these were: (a) failure of the transmitter to lock properly, (b) error in the aiming of the antenna with respect to the point being observed, or (c) incorrect doppler and libration shift during the centering process. As a positive check on the adequacy of each transmission, a written log was kept pulse-by-pulse and only those pulses listed as having met the various criteria were considered in the analysis.

Operations were undertaken only under conditions of clear skies or scattered light clouds. Figure 6 indicates the meteorological data recorded at Hanscom Air Force Base, approximately 1 mile distant, during the periods of observation in May 1963. For lack of direct measurement either during this period or under similar weather conditions, the zenith-path atmospheric absorption was extrapolated from previous observations and estimated to be 0.3 db one way.[6]

IV. DATA REDUCTION

Figure 7 shows a typical record of a single pulse with relatively high signal-to-noise ratio, as observed on the analog recording. The digital printout effectively noted the voltage at 0.5-second intervals but, because of the wider bandwidth, with slightly more noise. In order to allow a better estimate of the received power, the signal-to-noise ratio was improved by manually averaging the curves from 20 to 40 pulses for a single selenographic position. Figure 8 shows 3 samples of such curves, each representing the mean for a single series. The characteristic 2.5-second rise and fall of the integrator can be seen clearly in the stronger echo.

TABLE I

RADAR AND PROPAGATION PARAMETERS

Parameter	Value
Frequency	34,990 Mcps
Wavelength	8.57 mm
Peak power	12.0 w
Effective pulselength	2.5 sec
Receiver	
Mixer noise temperature	3300°K
Noise figure	10.9 db
IF bandwidths	
Monitor-analog record	170 cps
Data-digital record	250 cps
Video integration	2.5 sec
Stabilities	
Combined stability of local oscillator and transmitter	<100 cps/2.5 sec
Libration spread across half-power beamwidth	82 to 131 cps
Losses	
Plumbing; two-way	3.8 db
Estimated mean atmospheric on zenith path; two-way	0.6 db

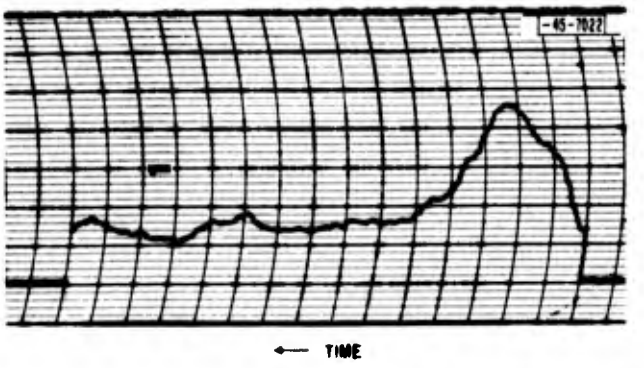

Fig. 7. Analog recording of single pulse returned.

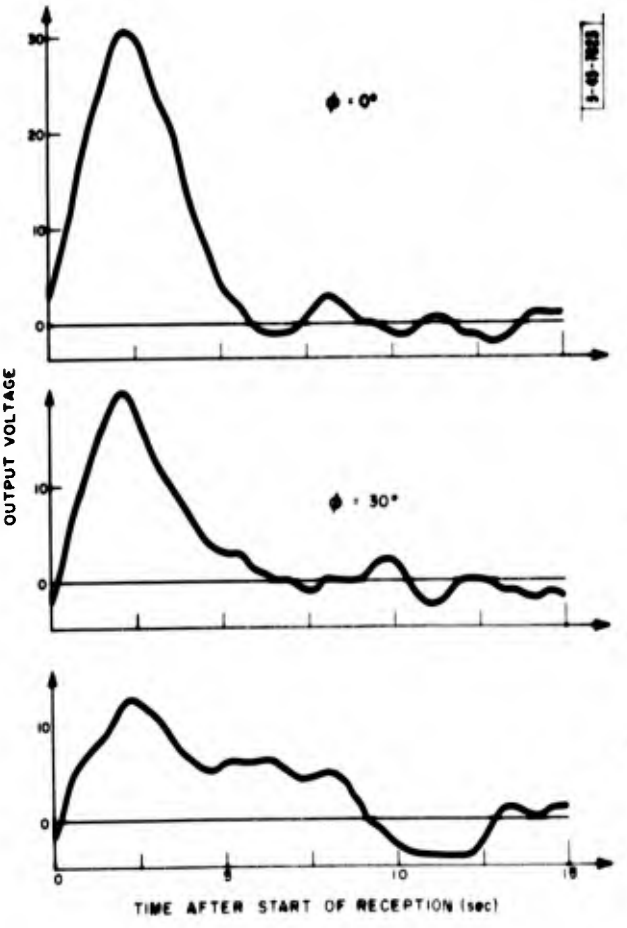

(a) Antenna directed at lunar center.

(b) Antenna directed halfway from center to limb.

(c) Beam center aimed at limb of moon.

Fig. 8. Mean responses for three different locations on the moon.

The baseline of the mean curve was determined by averaging all data points after 7 seconds. This period was chosen to insure the absence of signal in the integrator discharge. The value of the peak deflection above this baseline was used then to further describe the results for each series. Because the receiver gain varied, primarily with the doppler correction frequency, it was necessary to normalize the gain. In the absence of change in the noise figure the DC component is equivalent to the baseline level determined above and all data were thus normalized to a common base level.

The various calibration series were treated in an identical manner. A plot of the normalized calibration responses indicated no significant time-variant trends. For this reason, all voltages corresponding to a particular input power level were averaged and the resultant curve used for comparison with the lunar data.

Finally, the values for each series, now in terms of power, were corrected for beam pattern and atmospheric attenuation. The derivation of the pattern normalization factor is described later in this section. The atmospheric absorption, based on the mean elevation angle for the series, was taken to be the product of the cosecant of the elevation angle and 0.60 db, the estimated two-way zenith loss.

The position associated with the center of the beam for each series was then derived as described in Appendix B. However, the actual observations relate to a distribution about the beam center which depends on the directivity pattern and the lunar scattering laws. The antenna pattern is well known and, as a first approximation, it was assumed that the Lommel-Seeliger Law* applied and that each element of projected area reflected equally. In this simple case it is reasonable to describe position in terms of the point intercepted by the center of the beam, if this point is on the moon and more than one beamwidth from the limb. If, however, the beam center is near the edge of the lunar disk, it is clear that the position derived as above is invalid. In these cases, the portion of the beam pattern intercepting the disk was integrated in terms of gain and solid angle to determine the weighted center of scattering. This effective mean value of ϕ, the angle off-normal incidence to the mean sphere, is given for such cases. In all instances, however, the selenographic latitude and longitude coordinates given will be those corresponding to the center of the beam.

By numerical integration similar to that used in radiometric studies[6] the effective cross section observed was related to the total radar cross section of the moon.† In the same manner, the beam-pattern normalization factors were derived for positions near the lunar limb. In both cases, the radar uniform-brightness law was again assumed to describe the scattering. The results of this integration indicate that each observation, after application of the beam normalizing factor, represents the reflection at peak antenna gain from an equivalent projected area of $0.0151\ \pi a^2$, where πa^2 is the geometric cross section of the lunar disk. It should be emphasized that the normalized powers measured in this experiment refer to elements of equal projected area as opposed to the more common equal surface areas directly observed by range resolving radars.

In determination of the mean lunar scattering characteristics, the observed cross section is related to the applicable value of the angle ϕ. As stated above, both the value of ϕ for each

---

*The Lommel-Seeliger Law is characterized by equal reflected power from each element of projected area over the region for which the law applies.

†In this case the two-way pattern taken from Fig. 4 was used.

observation and the corrections for beam pattern were based on the assumption that all elements of the projected disk scatter equally. An examination of the data indicates that this is probably not strictly the case although the deviation is not great in regions which would significantly affect the calculations described. However, these two factors (value of ϕ, correction for beam pattern) should be re-derived for the actual scattering law observed to provide a more precise determination. This has not been done in the present analysis since, (a) the scattering law cannot be determined exactly from these data, and (b), the error involved is quite small compared with other uncertainties created by the low signal-to-noise ratio and limited number of observations.

V. RESULTS

The experimental results, processed as described thus far (essentially the least-reduced, usable form) are presented in Table II and directly plotted against a function of $\cos \phi$ in Fig. 9. Because the powers represented are related to observations of equal projected areas, the Lommel-Seeliger (uniform brightness) Law is given in Fig. 9 by a horizontal line of constant power.

The typical standard deviation shown is the estimated value associated with any one point plotted. This was derived by calculating the estimated standard deviation from the mean of each time-point in a series, and then averaging these values for all times of the mean response curve. Several series were thus treated and the value shown represents the average of those calculated.

The scatter of the points of Fig. 9 is not consistent with the noise of the data as indicated by the typical error bars. The most apparent discrepancy is represented by the points numbered 13, 14, 16 and 17, all much lower than the average of other values. The considerably lower power observed for these positions could reasonably be attributed either to an actual departure from the mean-scattering law or to erroneous measurement. It is indeed suspicious, however, that the group of series numbered 12 through 17 were observed consecutively in time without interruption by a calibration series, and in each case yield a power lower than all other observations at comparable values of ϕ. In addition, series numbered 14 and 60 (differing by almost 4 db in observed power) overlap to a considerable extent in specific terrain. The 12 to 17 group was taken approximately along a radial line from the lunar center, passing just north of the craters Copernicus and Aristarchus and includes varied terrain conditions. There appears to be no reason to suspect that the consistently lower values are a result of actual deviation from the mean-scattering law. Because of this it is assumed that, for some reason not evident from the experimental records (probably equipment malfunction) the data from groups 12 through 17 are in error.

The results were next collected in groups of closely related values of ϕ and the data in each group averaged. Figure 10(a) indicates the mean values for consideration of all points plotted in Fig. 9. The error bars represent the estimated standard deviation of the mean values. In Fig. 10(b) the treatment is identical except that the values for series 12 through 17 have been excluded. For the reasons given above, Fig. 10(b) is felt to represent the results more accurately.

In order to compare these results with those reported at lower frequencies, as measured with short-pulse radars, it is desirable to convert to the equivalent powers which would have been observed in measurement of equal surface areas. Since there are $\sec \phi$ units of surface area per unit of projected area, this is accomplished by multiplying each value of each power by the corresponding value of $\cos \phi$. Figure 11 presents the data of Fig. 10(b) replotted in this fashion

TABLE II

NORMALIZED DATA*

Series Number	Normalized Power Level Observed (all corrections applied) (10^{-18} watts)	Receiver Gain Normalizing Factor Used	Extinction Correction Factor (two-way) Used	Beam Pattern Normalizing Factor Used	Corrected ϕ (deg)	Selenographic Latitude (deg)	Selenographic Longitude (deg)
11	2.50	1.02	1.28	1	0.1	6.2 S	1.2 W
12	2.04	0.93	1.28	1	9.7	1.7 N	4.4 E
13	1.59	0.96	1.25	1	19.6	8.9 N	11.3 E
14	1.01	1.01	1.25	1	30.2	15.6 N	19.8 E
15	1.74	1.00	1.25	1	42.0	21.7 N	30.9 E
16	0.68	1.01	1.23	1.03	53.4	25.2 N	43.3 E
17	0.12	0.97	1.23	2.36	65.0	29.0 N*	90.0 E*
19	2.16	0.90	1.25	1	0.1	5.8 S	1.0 W
20	2.09	0.94	1.25	1	0.1	5.8 S	0.9 W
21	3.27	0.79	1.28	1	9.6	3.8 S	8.7 E
22	3.44	0.68	1.32	1	19.6	5.0 S	19.1 E
23	1.97	0.82	1.35	1	30.3	6.6 S	29.8 E
24	1.80	0.72	1.42	1	42.3	8.6 S	41.9 E
25	1.30	0.70	1.46	1.05	57.2	9.9 S	57.1 E
26	3.54	0.86	1.72	1	0.9	6.4 S	0.3 E
34	4.92	0.65	1.44	1	0.5	5.7 S	0.4 E
35	4.14	0.75	1.42	1	9.3	14.2 S	4.5 W
36	4.35	0.83	1.39	1	19.3	22.4 S	10.4 W
37	3.65	0.89	1.35	1	29.9	30.4 S	18.2 W
38	2.62	0.94	1.32	1	41.9	37.4 S	29.9 W
39	2.19	0.98	1.30	1.04	56.6	44.3 S	47.3 W
40	2.17	1.02	1.30	2.36	65.0	51.0 S*	90.0 W*
41	2.86	0.99	1.30	1	0.3	5.8 S	0.5 E
42	2.18	0.69	1.28	1	7.6	12.1 S	4.5 E
49	5.10	0.93	1.56	1	1.5	0.9 S	7.2 E
50	3.22	0.94	1.51	1	20.3	18.1 S	15.9 E
51	2.70	0.96	1.46	1	30.8	28.1 S	19.6 E
52	1.71	1.00	1.44	1	42.5	40.0 S	22.2 E
53	2.03	1.02	1.42	1.05	57.0	54.0 S	28.4 E
54	1.57	1.05	1.42	2.36	65.0	66.7 S*	90.0 E*
55	1.74	1.05	1.39	1.05	57.0	56.2 S	18.5 E
56	2.96	1.05	1.39	1	28.7	28.4 S	10.9 E
57	2.03	1.05	1.39	1	27.7	21.5 S	11.7 W
58	2.14	1.06	1.39	1	43.0	42.3 S	15.1 E
59	1.89	1.04	1.42	1	29.0	7.5 N	34.3 E
60	2.42	1.02	1.44	1	23.6	13.1 N	26.1 E
61	3.38	0.96	1.44	1	1.7	0.7 N	8.0 E
62	4.33	1.03	1.46	1	1.7	0.7 N	8.0 E
63	2.99	0.99	1.51	1	40.0	39.2 S	1.6 W
64	1.95	0.96	1.54	1	32.1	31.7 N	10.4 E

* Points for which the beam was actually slightly off the moon are shown with 90° longitude and the latitude of the nearest limb.

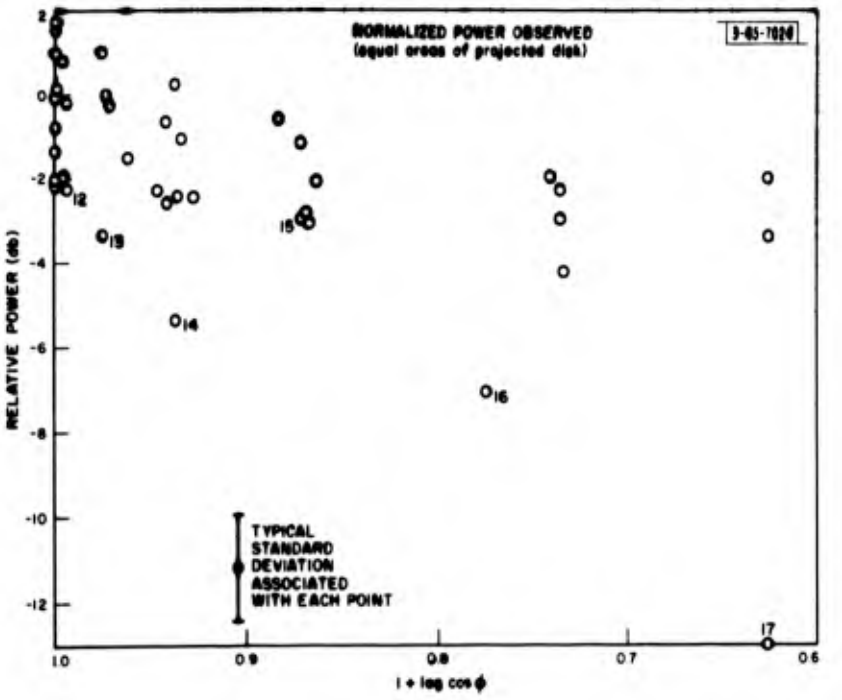

Fig. 9. Relative power observed for each position of observation showing all data of Table I.

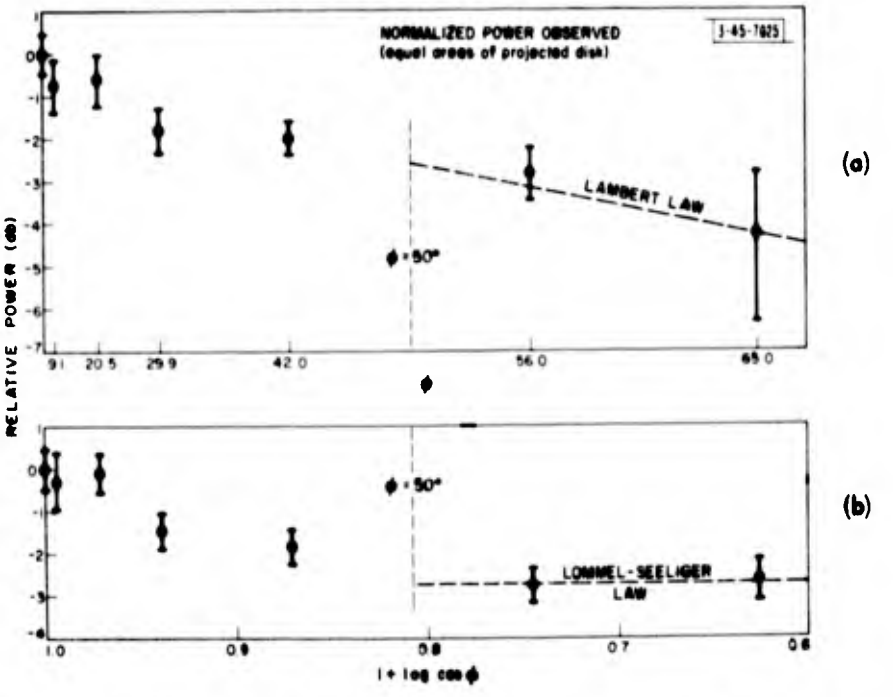

Fig. 10. Mean values of power observed: (a) for all data; (b) excluding the series 12-17.

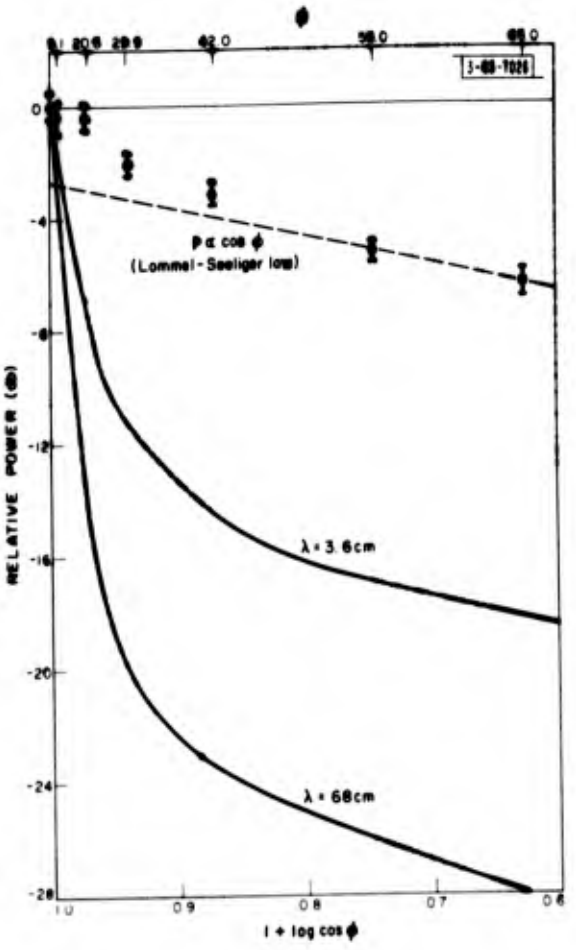

Fig. 11. Data of Fig. 10(b) replotted as a function of surface area with the 3.6- and 68-cm data for comparison.

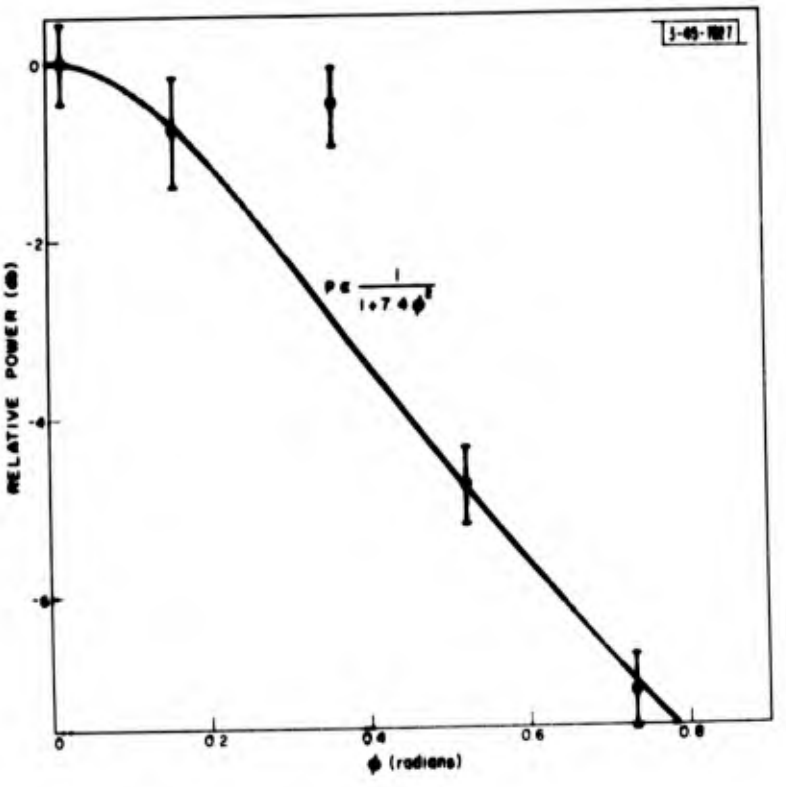

Fig. 12. Remainder after subtraction of the cos ϕ curve attributed to diffuse scattering.

and for comparison indicates the comparable 3.6- and 68-cm results reported by Evans and Pettengill.[5]

It is apparent from this plot that there is a marked difference in scattering between centimeter and millimeter wavelengths and that the specular component, so prominent at lower frequencies, is relatively unimportant at 8.6 mm. Unfortunately, the distribution and quantity of positions observed are insufficient to accurately define the contribution from each component.

The results reported at 3.6 cm indicate that beyond a value of $\phi = 50°$ the quasi-specular component provides no significant contribution and the observed power follows the Lommel-Seeliger Law. In the millimeter data there are results for only two values of ϕ in this region. These results closely fit a $\cos\phi$ curve as shown in Fig. 11. Therefore, if this curve is assumed to define the diffuse scattering component and is subtracted from the observations, the remainder can be attributed to quasi-specular scattering.

Figure 12 indicates the relationship of the data after this subtraction. At lower frequencies, many observers have been able to reasonably fit the results of specular scattering to an empirical expression of the form $P \propto \exp[-A \sin\phi]$. The data of Fig. 12 deviate radically from any curve of this form but are approximated most closely when the exponent A is slightly less than 3.

Evans and Pettengill[5] report a more precise fit to their data from another empirical expression

$$P \propto \frac{1}{1 + b\phi^2}$$

where the values of b were found to be 460 and 50, respectively, at 68- and 3.6-cm wavelengths. A curve of this form with b = 7.4 is shown in Fig. 12 and fits all but one point remarkably well. However, there appears to be no reason to assume that point to be in error and this neat result is attributed, pending further experimentation, to coincidence.

The total radar cross section of the moon can be found by relating the integrated beam pattern and the observed effective cross sections as described earlier. Since the sum of the curves of Figs. 11 and 12 fits the actual observations quite well, these curves were assumed to be valid in the computation of cross section. For reasons similar to those put forth in the previous discussion, the resulting values of cross section attributed to each component are highly uncertain but the sum of the two (the total lunar radar cross section) is much less so.

The straightforward computation of the diffuse component is described in a preceding section and yields a value of $0.058\ \pi a^2$. The total due to quasi-specular scattering is found, by numerical integration, to be $0.010\ \pi a^2$. Thus, the total lunar cross section at 8.6 mm is determined to be 7 percent of the geometric cross section. The following factors contribute to uncertainty in this value:

(a) Statistical variations in the averaged data (±12%)
(b) Statistical variations in the averaged calibration values (±10%)
(c) Uncertainty in the absolute power level of calibration signals (±15%)
(d) Uncertainty in the measurement of antenna gain (±12%)
(e) Uncertainty in the measurement of RF losses (±3%)
(f) Error in the estimate of atmospheric attenuation (±5%)
(g) Error in the determination of transmitted power (±5%)
(h) Uncertainty in the measurement of integrated bandwidth (±5%)
(i) Approximations used in analysis (±5%).

As these are all random in nature and are expected to have no bias effect, the over-all uncertainty is estimated to be ±27 percent, derived by taking the square root of the sum of the squares of the various contributions.

VI. CONCLUSIONS

The total radar cross section of the moon at 8.6-mm wavelength was found to be 7 ± 2 percent of the geometric cross section with approximately 85 percent of the reflection resulting from diffuse scattering. This corresponds closely with the meter and decimeter wavelength values reported but is at variance with several measurements in the centimeter band. The reader is referred to Table I and Fig. 1 of Ref. 7 for a presentation of previously reported results.

It is clear that at 8.6 mm the principal source of reflection is diffuse scattering with only a small contribution from the quasi-specular component. While the results can be reasonably interpreted in terms of the Lommel-Seeliger Law, there are insufficient data in these preliminary measurements to justify this as a conclusion.

In a thorough experimental program, one would desire to first establish the mean-scattering law by combining a large number of observations from many positions and then isolate terrain features which consistently deviate from this mean. With the limited sample reported herein, this was not possible. However, of the positions observed (each representing the integrated effect of all elements within the antenna beam) no valid observation appears to depart from the mean by more than about ±2 db. Within these limits, no distinction could be made between the maria and the continents.

ACKNOWLEDGMENTS

Our project has excited the interest of many members of the staff of Lincoln Laboratory and we have benefited much from their suggestions and assistance. We wish to particularly acknowledge the contributions of Jerome Freedman and James W. Meyer who played major roles in the initial conception of this project and have provided a continuing interest and enthusiastic support. We are grateful to W. W. Ward for much helpful guidance and aid. Special mention is due K. J. Keeping and his associates for the development of the antenna feed and assistance in measurement of the antenna parameters, C. M. Steinmetz who developed the phase-locked transmitter, J. H. Chisholm and Regina Shaputnic for the great assistance rendered in the reduction of data, J. A. Ball and Julia H. Dinsmore for extensive aid in computations and many members of the staff of the Engineering Division under J. F. Hutzenlaub who have made major contributions in several areas. The suggestions and encouragement of J. V. Evans are much appreciated.

APPENDIX A
OPERATION OF THE RADAR SYSTEM

A simplified block diagram of the radar system is shown in Fig. A-1. The major functional subdivisions will now be discussed.

I. BASIC MULTIPLIER

The fundamental frequency reference for the radar is provided by the basic multiplier, operating from a crystal oscillator at approximately 11.4 Mcps. The oscillator, first doubler and associated buffers and filters are carefully isolated from mechanical, thermal, magnetic, and high-frequency electric disturbances. The conceptual requirements are such that changes which are negligible over a period of 2.5 seconds are of no consequence. The stable 22.8-Mcps signal at a level of about 25 mw is then amplified and multiplied to X-band (approximately 8750 Mcps) in a solid-state varactor built by Microwave Associates. The 150-mw output is amplified by a V-27-B, two-cavity klystron to the half-watt level. At this point, a sample is extracted and supplied to the transmitter system as a reference frequency. The remainder is quadrupled in another Microwave Associates varactor unit to directly produce the receiver local-oscillator power at a frequency of approximately 35.030 Gcps.

II. TRANSMITTER

The transmitter is basically a klystron, phase-locked to the frequency of the local oscillator with a precise 30-Mcps offset derived in the locking process. A sample of the output of the Elliott Bros. nominal 10-watt, floating-drift-tube klystron oscillator is harmonically mixed with the X-band reference signal from the basic multiplier to produce a 30-Mcps difference frequency. This is then used to generate error signals in a combined phase and frequency correcting loop for the coarse (or long-term) and the fine controls, respectively. The resulting combined-error signal is applied to vary the beam current of the klystron. A detailed description of this transmitter system has been given by Steinmetz.[8] The final result is a precise frequency difference between the transmitter and local oscillator which is exactly defined by the frequency of the phase detector reference oscillator (30 Mcps).

III. TEST MULTIPLIER

Since the operation of this low-power system hinges on precise frequency control and the resulting ability to utilize very narrow bandwidths, it is imperative that the over-all stability be continuously monitored. For this reason, a second multiplier chain (similar to that of the basic multiplier) was constructed with its output at X-band approximately at the fourth subharmonic of a frequency 30 Mcps below that of the transmitter (or 60 Mcps below the local oscillator). This X-band signal is harmonically mixed with a sample of the transmitter output, amplified at about 30 Mcps, mixed to a lower frequency and displayed on a high-resolution spectrum analyzer. For obvious reasons, the more stable of the two chains was chosen for the basic multiplier. Therefore, the greater contribution to the observed spectral impurity could readily be attributed to the test multiplier. The width of the resulting spectrum, observed over a 15-second period at the rate of one sweep per second, is less than 100 cps.

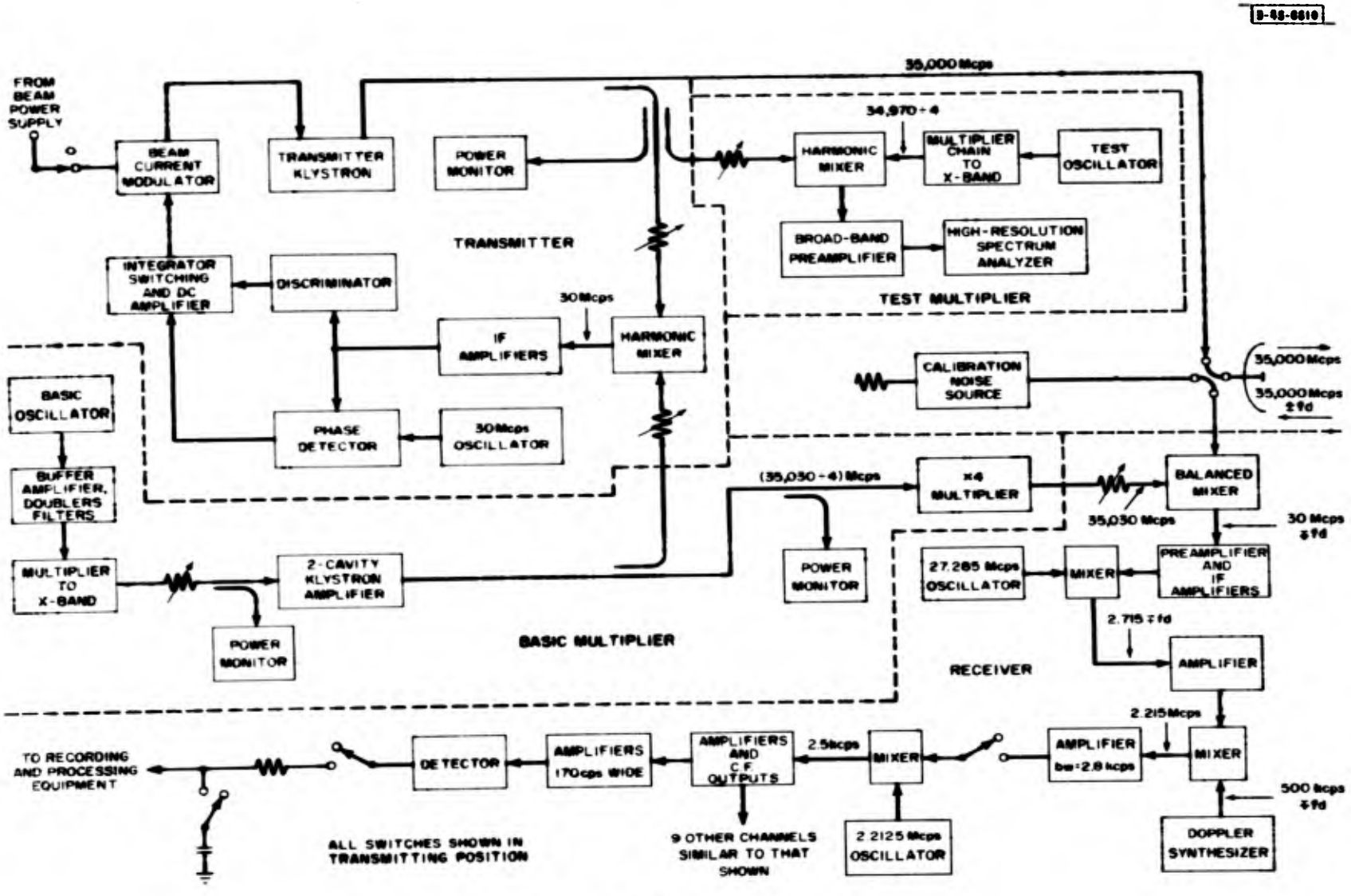

Fig. A-1. Pseudo-CW radar system.

IV. RECEIVER

Before describing the actual receiver, it seems desirable to briefly review the lunar characteristics which affect the signal in the frequency domain and to define some terms used herein.

The distance to the lunar center will vary, with time as a function of earth rotation and the orbit of the moon. The frequency shift associated only with this radial motion will be called by the customary term "doppler shift." In addition, the moon appears to an observer on earth to revolve about its center. For a radar with a wide antenna beam, this motion or libration has the effect of smearing the transmitted spectrum as the various scattering elements have different radial components of velocity. With a narrow antenna beam, only a portion of the surface is examined. The scatterers within the beam again have differing radial-velocity components which smear the spectrum as in the wide-beam case but to a lesser extent since the velocity distribution is smaller. The effective frequency spreading within the beam is herein called the "libration smearing." In addition to this spreading, however, there is a shift of the center of the spectrum or the equivalent of a frequency bias due to the rotational motion. This will be called the "libration shift."

The notation f_d in Fig. A-1 applies only to the doppler shift. Although it is not indicated on the diagram, the notation plus or minus libration shift should be carried on all receiver frequency designations, including those following the correction for doppler. Thus, the frequencies of the diagram are correctly labeled for only the special case where the center of the antenna beam is directed at a point on the libration axis of the moon.

During the receive period, the antenna is connected to the balanced mixer, and the incoming signal is heterodyned with the output of the basic multiplier to produce the first IF of 30 Mcps (except as modified by lunar motions). The following mixing changes the nominal IF to 2.715 Mcps. This signal is further mixed with a doppler correction frequency of 500 kcps modified by the computed doppler shift after which, assuming the insertion of appropriate doppler corrections, the signal frequency is precisely 2.215 Mcps except for possible libration shift.

The doppler correction is quantized in 50-cps steps. From computer printouts, a 5-digit binary tape is prepared which represents, to the nearest 50 cps, the change in doppler frequency in each 5-minute period. A series of clutches and differential gears driven by the tape reader then mechanically performs the precise linear interpolation to create a chain of output pulses – each pulse ordering a 50-cps change in frequency. These pulses operate on three oscillators of 10 crystals in 50-cps steps, 10 in 500-cps steps, and 30 in 5-kcps steps, respectively, and advance them appropriately. The three are heterodyned in a series of mixing and filtering operations to produce the 500 ± 75 kcps.

The 2.215-Mcps IF, now corrected to remove the doppler shift, is amplified with a bandwidth of approximately 3 kcps, then mixed to a center frequency of 2.5 kcps to permit simple construction of narrow-band filters. The frequency characteristics of the signal at this point are defined by the following.

Spectral Width:– The combination of transmitter and local oscillator instabilities over a 2.5-second period (transit time for moon path) and the libration spreading, which may be 0 to 150 cps at the antenna 3-db points, are the main factors of this component. The instabilities produced by the receiver heterodyning oscillators below 30 Mcps are negligible.

Displacement from Nominal Center Frequency:– Three contributions to this component are present: (1) error in doppler correction; (2) the maximum of 25-cps error introduced by 50-cps

quantization of the doppler correction; and (3) the libration shift which is dependent on libration rate and the position of the beam on the moon, up to approximately 500 cps in either direction.

The 2.5-kcps IF is directly recorded on magnetic tape. This provision was made to permit replay with varying forms of narrow-band units, integrators and detectors in order to increase the probablity of detection. As used, it served no practical purpose in the measurements program.

As a monitor of the frequency domain, 10 narrow channels, each with a bandwidth of 170 cps to accommodate the anticipated spectral width, are spaced 100 cps apart. The outputs of these overlapping filters are square-law detected, integrated and displayed on a multichannel, analog pen-recorder. Thus as the libration shift varies, the signal can be expected to appear in different channels, the entire possible band being covered.

For observations of a particular area of the lunar surface, the libration shift is computed approximately and checked against the frequency displacement of the channel in which signal appears. Then a correction of this amount is superimposed on the doppler correction causing the signal to appear in the central filter. A separate receiver channel, with a bandwidth of 250 cps and center frequency coincident with that of the central monitor channel, is then used as the source of actual data. This bandwidth is adequate to insure the inclusion of the entire spectrum of the received signal. The detected and integrated output of this filter is recorded by a Hewlett-Packard digital voltmeter and printer.

V. DUPLEXING AND DUTY CYCLE

For the purpose of simple detection, the most desirable form of operation of this system is the transmission of a 2.5-second pulse. This is followed by reception for a period adequate to permit the charge and discharge of the integrator circuit (about 5 seconds) and to indicate the receiver baseline by observation of signal-free noise for some additional interval. With no attempt to measure range or to provide range resolution, the 2.5-second CW pulse contains the maximum energy possible in this time period equivalent to the two-way lunar range. This low-frequency operation permits the use of a mechanical waveguide switch for duplexing, the switching requiring approximately 100 msec. A 4-port waveguide transfer switch performed this basic duplexing function.

If the transmitter were permitted to remain in operation during the receive period, it would be necessary to provide an isolation of approximately 210 db. Because of the difficulty of achieving this, in spite of frequency shifting and switching, it is necessary to stop the oscillation of the phase-locked klystron during the receive time. This is accomplished by removing the beam voltage from the tube in synchronism with the operation of the waveguide switch. This in turn, however, creates additional problems. Since the tube is tightly phase-locked in a relatively narrow-band circuit, the removal of beam voltage causes the tube to cool and, upon resumption of oscillation, the open-loop oscillator frequency is well outside the capture range of both the AFC and APC loops. For this reason, it is necessary to transmit for a period longer than the desired 2.5 seconds with the following sequence of events: (1) when the tube is turned on, it oscillates in a free-running condition; (2) when the open-loop frequency enters the capture range due to thermal tuning, the oscillator is phase-locked; and (3) it must remain locked for at least the desired 2.5 seconds. All transmitted energy, both locked and unlocked, which is radiated prior to the last 2.5 seconds before the receiver is connected is wasted.

For this reason, the actual duty cycle used is 15 seconds of transmit time and 15 seconds of receive period, the wasted transmitter energy serving only to decrease the data rate.

In addition, because of the integrators, it is necessary to isolate the later stages of the receiver during the transmission period to prevent a build-up of integrator charge due to RF leakage. This is readily done by switching in the IF lines. Since the receiver front-end noise without signal produces a DC bias on the integrating capacitor, the removal of this noise by opening the IF path causes the integrator to discharge toward the no-voltage level; thus it is also necessary simultaneously to isolate the capacitor from its discharge path during the transmission interval. The various switches involved in the over-all duplexing process are functionally indicated in Fig. A-1.

VI. CALIBRATION FACILITIES

The basic radar parameters are measured in absolute terms before and after each test. During the observations each parameter is monitored in a relative sense to insure that there is no unobserved change.

The fundamental output of this radar is the level of reflected power observed. Only amplitude measurements are possible with this initial system. The calibration of this level is slightly complicated by the invariably negative signal-to-noise ratios prior to the video integration process and by the very narrow IF bandwidths (approximately 0.000 000 5 percent). Under these conditions, the only practical signal source capable of producing accurate signal levels within the bandpass is a noise generator. A carefully calibrated variable attenuator and a neon-discharge noise tube are connected to one port of the waveguide switch. With the transmitter disabled, the receiver is switched from the noise source to the antenna at the normal duty rate. The various switching processes in the receiver are reversed so that the normal "receive" operation now takes place when in the "transmit" position with the receiver connected to the noise source. While the receiver is connected to the antenna, the noise source is turned on but contributes to the signal input only after the waveguide switching. At a precisely controlled time after the switching is affected (nominally 2.5 seconds), the noise tube is switched off.

In this manner, an accurately determined power level (dependent on the IF bandwidth) is received for a period equal to that of the lunar signal. The resulting deflection of the output voltage, recorded in the same manner as the moon data, can be directly compared with the actual measurements to establish levels of received power.

APPENDIX B
DEFINITION OF LUNAR POSITIONS

The grossest feature of the moon is obviously its nearly spherical shape. The reduction of radar data, therefore, should first attempt to define the mean scattering function of the lunar surface or the variation in backscattered power as a function of the angle of incidence to the mean sphere. Having once adequately established this average response, it would then be desirable to describe the reflections with respect to the finer lunar features. In this case, the position associated with each observation must define a specific selenographic terrain feature.

During the experiments, the position of the center of the antenna beam was recorded with respect to a rectilinearly gridded reticle in the optical boresight system. In effect, the subtended angles between the beam center and the nominally horizontal and vertical tangents to the lunar limb were noted. These are respectively defined as $\Delta\epsilon$ and ΔZ as indicated in Fig. B-1(a).

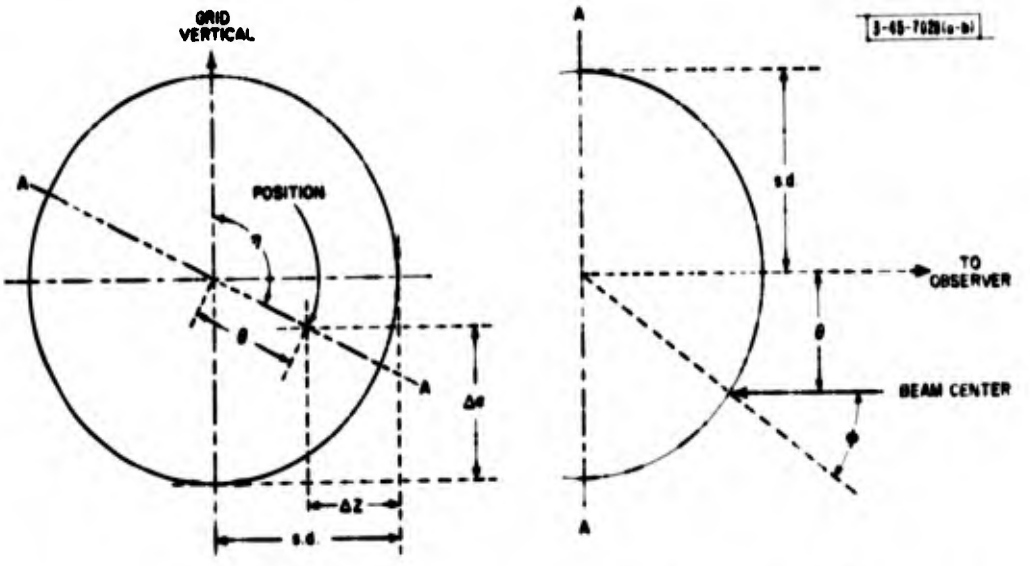

(a) Apparent disk.

(b) Disk in plane of A-A and center.

Fig. B-1. Basic geometry of lunar positions.

The angle ϕ, defined as the angle between normal and actual incidence to the mean sphere, is used to describe the average scattering function. Figure B-1(b) indicates its relationship to the grid-recorded angles. Then, from Fig. B-1,

$$\Theta = \{[(\text{s.d.}) - (\Delta Z)]^2 + [(\text{s.d.}) - (\Delta\epsilon)]^2\}^{\frac{1}{2}}$$

and

$$\phi = \sin^{-1}\left(\frac{\Theta}{\text{s.d.}}\right)$$

where Θ is defined in the diagram as the subtended angle from the apparent center to the position considered and s.d. is the semidiameter as tabulated in the American Ephemeris.

The specific designation of position with respect to lunar features is given in terms of selenographic latitude and longitude following the conventions of the American Ephemeris and Nautical

Almanac for 1963. (Mare Crisium is in the northwest quadrant and Mare Nubium is in the southeast.) Most of the conversion can be readily accomplished by specifying the position in polar coordinates with radius θ and angle η shown in Fig. B-1. The angular polar origin is first corrected for the difference between grid-vertical and true-vertical which in this case, because of misalignment of the reticle, was approximately 10°. Then the angle between terrestrial and astronomical coordinates, μ, is added algebraically. This is the angle between true-vertical and the declination circle through the position and is given as a function of actual azimuth Z as

$$\mu = \sin^{-1}\left\{\frac{\sin Z \cos \ell_o}{\cos \delta}\right\}$$

where ℓ_o is the observer's latitude and δ is the declination of the position observed. Finally, the angle is corrected by the position angle of the lunar axis (i.e., the angle between the declination circle and the lunar N-S axis) which is tabulated in the American Ephemeris. At this point, the position is expressed in terms of polar coordinates with the origin at the center of the apparent disk and with angles measured from a radius which passes through the north selenographic pole.

If, for the moment, the apparent center is defined as the origin in an apparent selenographic latitude and longitude system with the north pole at the intersection of the limb and the origin of the polar-coordinate angles described above, the position considered may be readily converted to terms of its apparent latitude ℓ_A and apparent longitude λ_A. In a final step, the rotation of the lunar sphere must be considered. The American Ephemeris tabulates the true selenographic latitude ℓ_e and longitude λ_e of the point where the line between earth and moon centers intersects the lunar surface (sub-earth point). This point, except for a small parallax correction when the moon is not at the observer's zenith, is the origin of an arbitrary system of apparent latitudes and longitudes. Then, from spherical trigonometric derivations, the actual selenographic latitude ℓ and longitude λ are given by:

$$\sin \ell = \sin \ell_A \cos \ell_e + \cos \ell_A \sin \ell_E \cos \lambda_A$$

and

$$\sin(\lambda - \lambda_e) = \frac{\cos \ell_A \sin \lambda_A}{\cos \ell} \quad .$$

REFERENCES

1. E.S. Rosenblum, "Atmospheric Absorption of 10-400 kMcps Radiation: Summary and Bibliography to 1960," G-Report 82G-0021 [U], Lincoln Laboratory, M.I.T. (15 August 1960), DDC 242598, H-150.
2. V.L. Lynn, M.D. Sohigian and E.A. Crocker, paper presented at A.G.U. Meeting, Washington, D.C. (18 April 1963).
3. K.J. Keeping, "A Wide-Band Antenna, Having Axially Symmetrical Patterns High Gain and Low Side Lobes for All Polarizations," G-Report 46G-0008 [U], Lincoln Laboratory, M.I.T. (30 November 1960), DDC 248360, H-227.
4. W.D. Fitzgerald, V.L. Lynn and K.J. Keeping, "Experimental Evaluation of a 1000-Wavelength Antenna," G-Report 46G-4 [U], Lincoln Laboratory, M.I.T. (13 May 1963), DDC 406109, H-152.
5. J.V. Evans and G.H. Pettengill, J. Geophys. Res. 68, 423 (1963).
6. V.L. Lynn, M.L. Meeks and M.D. Sohigian, "Radiometric Measurements at 8.5-mm Wavelength with a 28-Foot Antenna During December 1962," Technical Report No. 330 [U], Lincoln Laboratory, M.I.T. (8 October 1963).
7. J.V. Evans and G.H. Pettengill, J. Geophys. Res. 68, 5098 (1963).
8. C.M. Steinmetz, "Precision Frequency Control of a High-Power Millimeter Klystron," Technical Report No. 253 [U], Lincoln Laboratory, M.I.T. (3 January 1962), DDC 273509.

UNCLASSIFIED